ACS APPLIED MATERIALS & INTERFACES

Research Article

www.acsami.org

Trifunctional Polymeric Nanocomposites Incorporated with Fe_3O_4/Iodine-Containing Rare Earth Complex for Computed X-ray Tomography, Magnetic Resonance, and Optical Imaging

Xin Wang,[†] Mengqi Tu,[‡] Kai Yan,[†] Penghui Li,[§] Long Pang,[†] Ying Gong,[†] Qing Li,[†] Ruiqing Liu,[†] Zushun Xu,*[,†] Haibo Xu,*[,‡] and Paul K. Chu*[,§]

[†]Hubei Collaborative Innovation Center for Advanced Organic Chemical Materials, Ministry of Education Key Laboratory for The Green Preparation and Application of Functional Materials, Hubei University, Wuhan, Hubei 430062, China

[‡]Department of Radiology, Union Hospital, Tongji Medical College, Huazhong University of Science and Technology, Wuhan, Hubei 430030, China

[§]Department of Physics and Materials Science, City University of Hong Kong, Tat Chee Avenue, Kowloon, Hong Kong, China

Supporting Information

ABSTRACT: In this study, a novel polymerizable CT contrast agent integrating iodine with europium(III) has been developed by a facile and universal coordination chemistry method. The Fe_3O_4 nanoparticles are then incorporated into this iodine-containing europium complex by seed-emulsifier-free polymerization. The nanocomposites combining the difunctional complex and superparamagnetic Fe_3O_4 nanoparticles, which have uniform size dispersion and high encapsulation rate, are suitable for computed X-ray tomography (CT), magnetic resonance imaging (MRI), and optical imaging. They possess good paramagnetic properties with a maximum saturation magnetization of 2.16 emu/g and a transverse relaxivity rate of 260 mM^{-1} s^{-1}, and they exhibit obvious contrast effects with an iodine payload less than 4.8 mg I/mL. In the in vivo optical imaging assessment, vivid fluorescent dots can be observed in the liver and spleen by two-photon confocal scanning laser microscopy (CLSM). All the results showed that nanocomposites as polymeric trifunctional contrast agents have great clinical potential in CT, MR, and optical imaging.

KEYWORDS: *computed X-ray tomography imaging, magnetic resonance imaging, rare-earth fluorescent, iodine-containing contrast agents, polymeric nanocomposites*

1. INTRODUCTION

Polymeric nanocomposites have gained much attention in recent years in biomedicine especially diagnostic imaging. They are used as contrast agents to enhance the imaging effect in magnetic resonance imaging (MRI),[1] fluorescent imaging,[2] computed X-ray tomography (CT),[3,4] and positron emission computed tomography (PET).[5]

CT is a common diagnostic tool to obtain high-resolution 3D structural details of tissues with high efficiency.[6] The patterns of CT are plain CT scan and contrast enhancement (CE). Until recently, the widely used CT contrast agents were mainly based on small iodine-containing molecules because of the large atomic number.[7,8] The clinically used small iodine contrast agents are classified as ionic (e.g., Angiografin, Urografin, and Hapaque) and nonionic (e.g., Omnipaque, Iopamiro, Ultravist, and Isovist). A major indicator is the iodine payload (mg I/mL). The same amount of contrast agent with a larger iodine payload shows better imaging effects. However, the small iodine contrast agents have a short circulation time and may cause side-effects in patients because of the different osmolality and viscosity. Hence, new contrast agents with higher contrast and smaller side effects are being devel-

Received: June 30, 2015
Accepted: October 20, 2015
Published: October 20, 2015

DOI: 10.1021/acsami.5b08802
ACS Appl. Mater. Interfaces 2015, 7, 24523−24532

oped.[9−14] For instance, de Vries et al. developed micelles as blood-pool CT contrast agents by combining 1,2-distearoyl-*sn*-glycero-3-phosphocholine (DSPC) with octan-2-yl 2,3,5-triiodobenzoate,[15] and deKrafft et al. used 2,3,5,6-tetraiodo-1,4-benzenedicarboxylic acid (I_4-BDC-H_2) bridging ligands and metal connecting points of Cu(II) or Zn(II) to develop the nanoscale metal−organic frameworks (MOFs) as CT contrast agents.[16] In addition, polymeric CT contrast agents that combine the small iodine contrast agent with a polymer by covalent bonding have some unique merits.[17] Aviv et al. synthesized iodine-containing copolymeric NPs P(MAOETIB-GMA) with the monomer of MAOETIB (HEMA and 2,3,5-triiodobenzoic acid incorporated) and glycidyl methacrylate (GMA).[18] Compared to the ordinary iodine-containing contrast agents, the polymeric CT contrast agents tend to obtain better imaging effects, lower toxicity, and longer blood circulation time. It is also relatively easy to incorporate functional groups into the polymeric CT contrast agents to produce multifunctional contrast agents.[9]

MRI is a powerful diagnostic technique providing non-invasive, high spatial resolution, and real-time detection of diseases.[19] On the basis of the relaxation in different directions (longitudinal and transverse), researchers have developed many different types of MRI contrast agents.[20−24] Superparamagnetic iron oxide nanoparticles (SPIONs) such as Fe_3O_4 and γ-Fe_2O_3 are significant T_2 contrast agents because of their controllable size, shape, and surface characteristics.[25−29] These superparamagnetic nanoparticles can deliver the desirable contrast effect at low concentrations and be rapidly cleared from organisms afterward. Besides, SPIONs have high relaxivity, good chemical stability, low toxicity, and biocompatibility rendering them to be suitable for the magnetic core in contrast agents.[30] In general, SPIONs tend to be swallowed by the reticuloendothelial system (RES) of healthy cells so that they can conveniently distinguish the tumors lacking effective RES from the surrounding healthy cells.[31]

Nanoparticles (NPs) with fluorescent properties are used as fluorescence probes to track target delivery and controlled-release delivery system.[32] Thereinto, lanthanides possess many outstanding properties such as photostability, unique narrow emission bands, long excited-state lifetime, large Stokes shift, and high quantum yield.[33,34] For example, the europium complex has gained tremendous research interest in lanthanide materials.[35]

To achieve higher diagnostic accuracy, researchers tend to combine the advantages of various imaging methods, for instance, CT/optical imaging,[2] MRI/PET,[36] and PET/CT.[37] The development of nanocomposites for multifunctional imaging diagnosis is of great clinical importance. Many prominent achievements of MRI/CT/optical imaging contrast agents have been reported. Xing et al. combined the up-conversion materials (NaY/GdF_4: Yb, Er, and Tm) with Au NPs to prepare trifunctional nanocomposites,[38] and Xiao et al. employed a similar method to combine gadolinium-ion-doped up-conversion nanoparticles with tantalum oxide (TaO_x, $x \approx 1$) to achieve triple functions.[39] However, the preparation method and decoration of up-conversion nanoparticles tend to be complex and expensive. It is thus of both scientific and technological interest to integrate SPIONs and rare-earth fluorescence with a small iodine contrast agent to produce multifunctional polymeric contrast agents, although reports on polymeric nanocomposites with polymerizable complexes containing iodine and rare earth elements have been rare. The use of lanthanide elements is another option to enhance the CT contrast;[40] in fact, the CT imaging effects are usually better for smaller iodine payloads.

We have recently reported the preparation of functional nanocomposites by integrating polymerizable fluorescent complexes with Fe_3O_4 NPs by means of two-step seed-emulsifier-free emulsion polymerization.[41] This nanocomposite, which has excellent fluorescent and magnetic properties, can be used as a contrast agent in MRI/optical imaging. In this paper, based on previous research, we report a new difunctional polymerizable CT contrast agents and a novel polymer nanocomposite with triple functionalities, namely CT, MRI, and fluorescent imaging, via a new, simple, and versatile method.

2. MATERIALS AND METHODS

2.1. Materials. Sodium diatrizoate hydrate (98%), europium oxide (Eu_2O_3, 99.9% metals), iron chloride hexahydrate ($FeCl_3{\cdot}6H_2O$), and iron chloride tetrahydrate ($FeCl_2{\cdot}4H_2O$) were purchased from Aldrich and used directly. Styrene (St), acrylic acid (AA), and glycidyl methacrylate (GMA) were purified by distillation under reduced pressure and stored at 5 °C. Potassium peroxydisulfate (KPS) was purified by recrystallization in distilled water and dried under vacuum. Oleic acid (OA), undecylenic acid (UA), hydrochloric acid (HCl), anhydrous sodium hydroxide (NaOH), ammonium hydroxide ($NH_3{\cdot}H_2O$, 25−28%), 1,10-phenanthroline (Phen), and absolute ethanol were purchased from Sinopharm Chemical Reagent Co., Ltd., China, and used without purification, and 3-(4,5-dimethyl thiazol-2-yl)-2,5-diphenyl tetrazolium bromide (MTT) was bought from Sigma-Aldrich.

2.2. Synthesis of Eu^{3+} Complex: $Eu(AA)_2(DTA)Phen$. The $EuCl_3$ solution in ethanol (0.1 mol L^{-1}) was prepared by a method described previously.[22] Sodium diatrizoate hydrate (1 mmol), AA (2 mmol), and Phen (1 mmol) were added to a two-necked flask and dissolved in 50 mL of ethanol. The mixture was stirred at 60 °C for 30 min, and 10 mL of the $EuCl_3$ solution was added slowly. The final mixture solution was stirred for 15 h and purified by filtering, washed repeatedly with ethanol at 60 °C, and dried in vacuum at 50 °C for 12 h.

2.3. Preparation of Fe_3O_4/Poly(St-GMA-$Eu(AA)_2(DTA)Phen$) Trifunctional NPs. Modification of Fe_3O_4 NPs with oleic acid and sodium undecylenate (Fe_3O_4/(OA/NaUA), solid content of 14 wt %) was performed by a common method.[41] The $FeCl_3{\cdot}6H_2O$ (23.1 g) and $FeCl_2{\cdot}4H_2O$ (10.3 g) were added into 80 mL of deionized water at 40 °C under mechanical stirring for 15 min. Then, 70 mL of $NH_3{\cdot}H_2O$ was quickly injected into the mixture solution under vigorous stirring for 30 min. The solution was heated to 70 °C for 1 h and Fe_3O_4 NPs were separated from it by a powerful magnet. The Fe_3O_4 NPs were then washed by distilled water to neutral. The purified Fe_3O_4 NPs were mingled with ethanol (50 mL) and distilled water (50 mL) and heated to 80 °C under stirring. A 4 g mass of OA was added into reactor, and the reaction was maintained for 1 h. The Fe_3O_4/OA NPs were magnetically separated from the mixture and excess OA was removed by multiple alcohol washings. The purified Fe_3O_4/OA NPs, 20 mL of chloroform, and 30 mL of an aqueous solution of NaUA (8 g) were added into the reactor under stirring at 40 °C for 2 h and sonicated for 30 min. Finally, the mixture was kept under stirring until its weight was no longer changing. Thus, the aqueous solution Fe_3O_4/(OA/NaUA) NPs were obtained. All the above experimental procedures needed a nitrogen atmosphere.

The trifunctional nanoparticles (TFNPs) were synthesized by seed-emulsifier-free polymerization. The aqueous solution of modified magnetic Fe_3O_4 NPs (4.5 g), St (2 g), GMA (0.3 g), and distilled water (40 mL) were added into a four-necked flask and mechanically mixed for 30 min at room temperature. The aqueous solution of KPS (0.1 g/5 mL) was added dropwise into the flask as the initiator. The system was heated to 75 °C under stirring. After reacting for 1 h, 5 mL of the $Eu(AA)_2(DTA)Phen$ (complex, 0.2 g) solution (1 mL DMSO and 4 mL deionized water) was added within 15 min, and the

DOI: 10.1021/acsami.5b08802
ACS Appl. Mater. Interfaces 2015, 7, 24523−24532

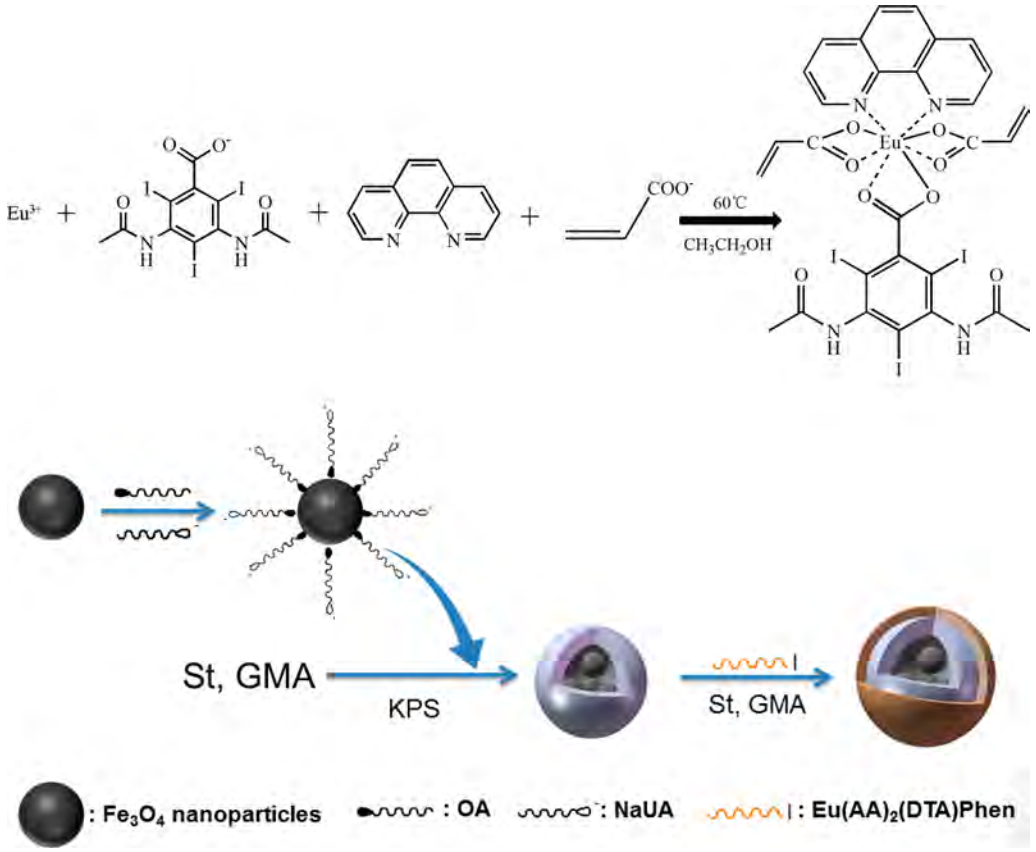

Figure 1. Schematic illustration of the preparation of $Eu(AA)_2(DTA)Phen$ and TFNPs.

polymerization reaction proceeded for another 4 h. The experiments were conducted in a nitrogen environment. The end product was dialyzed against distilled water (4−6 days, replenished every 8 h) for further purification. The solid sample was obtained by putting the saturated calcium chloride/methanol solution into latex. Then the precipitate was collected by centrifugation and rinsed with methanol and distilled water. This process was repeated several times, and the product was acquired by vacuum drying at 50 °C for 15 h.

2.4. In Vitro Cytotoxicity Test. The biocompatibility of the TFNPs was assessed by the MTT assay. The HeLa cells were seeded on 96-well plates (10^4 cells per well) and incubated in the DMEM culture medium at 37 °C and 5% CO_2 for 24 h. Half of the culture medium was removed, and DMEM containing different concentrations of TFNPs (dose diluted by complete medium, 0−1.8 mg/mL) was injected to every well. After incubation for 24 h incubation at 37 °C, all media was discarded, and PBS (pH 7.5) was used to wash cells several times. The MTT solution (30 μL, 5 mg/mL) was added to each well, and the cells were further incubated at 37 °C for additional 4 h. The MTT medium was discarded, and DMSO (200 μL) was added to each well. After dissolving the residual crystals, the optical density (OD) of the samples at 570 nm was obtained via microplate reader. The cell viability was assessed by the formula: viability = $(OD_{treated}/OD_{control}) \times 100\%$, where $OD_{treated}$ corresponds to the OD of experimental cells treated with TFNPs and $OD_{control}$ is the OD from control group without treatment.

2.5. In Vitro CT Characterization. To explore the effectiveness of the complex and TFNPs in CT imaging, the in vitro CT images were acquired on a Dynamic Volume CT (Aquilion ONE 640, Toshiba, Japan) with a tube voltage of 120 kV and current of 250 mA. The samples were diluted with distilled water on the basis of the iodine payload and transferred to a 0.5 mL centrifuge tube. The important instrumental parameters were: field of view = 90 mm × 140 mm, rot. time =1.0 s, and D-FOV = 220.3 s. The linear fit was based on the CT value (unit: Hounsfield unit, HU) and iodine payload.

2.6. In Vitro and in Vivo MRI Characterization. To confirm the relativity of MRI in vitro, the TFNPs were diluted with distilled water on the basis of the iron concentrations from 0 to 0.11 mmol/L. All samples were infused into a 0.5 mL centrifuge tube and placed in a clinical 3T MR scanner. The T_2 relaxation time of the latex was calculated by the software (MATLAB V7.1), and the relativity values of r_2 were plotted versus the linear fit between $1/T_2$ relaxation time and Fe concentration.

The in vivo MR imaging was carried out on Sprague−Dawley (SD) rats (weight of nearly 220 g). These experiments followed the protocols of the Institutional Animal Care and were approved by the Use Committee at Hubei University and the Institutional Animal Care. All rats were anaesthetized by trichloroacetaldehyde hydrate (10%) on the basis of weight (35 mg/kg) before the experiments. The in vivo scan was measured before and after tail vein injection of TFNPs solution with the concentration of 5.4 mg Fe/kg body weight. The images were obtained on the MR scanner using continuous time points. The signal intensity (SI) of the liver, spleen, kidney, and muscle was measured by system program from the T_2-weighted coronal MR images. The relative SI was calculated as follows: $SI_{pre}/SI_{post} \times 100\%$. The SI_{pre} and SI_{post} are SI measurements before and after injection of the TFNPs, and the SI_{post} values were measured at continuous times of 30, 60, 120, 180, and 300 min.

All MR images (in vitro and in vivo) were acquired at 25 °C on the 3.0T whole-body MR scanner (MAGNETOM Trio, A Tim System 3T, Siemens, Munich, Germany) in combination with an eight-channel wrist joint coil. The parameters of the in vitro MR were: field of view (FOV) = 120 mm, base resolution = 384 × 384, slice thickness = 1.5 mm, multiple echo times (TE) = 20, 40, 60, 80, 100, 120, and 140 ms, repetition time (TR) = 2000 ms, and scanning time = 13−14 min. In the in vivo MR, the FOV was 100 mm, base resolution was 192 × 192, slice thickness was 3.0 mm, TE was 62 ms, TR was 3000 ms, and flip angle was 120°.

2.7. Histological Analysis and Optical Imaging. The liver, spleen, kidney, and muscle of rats were removed 9 h after injection of

DOI: 10.1021/acsami.5b08802
ACS Appl. Mater. Interfaces 2015, 7, 24523−24532

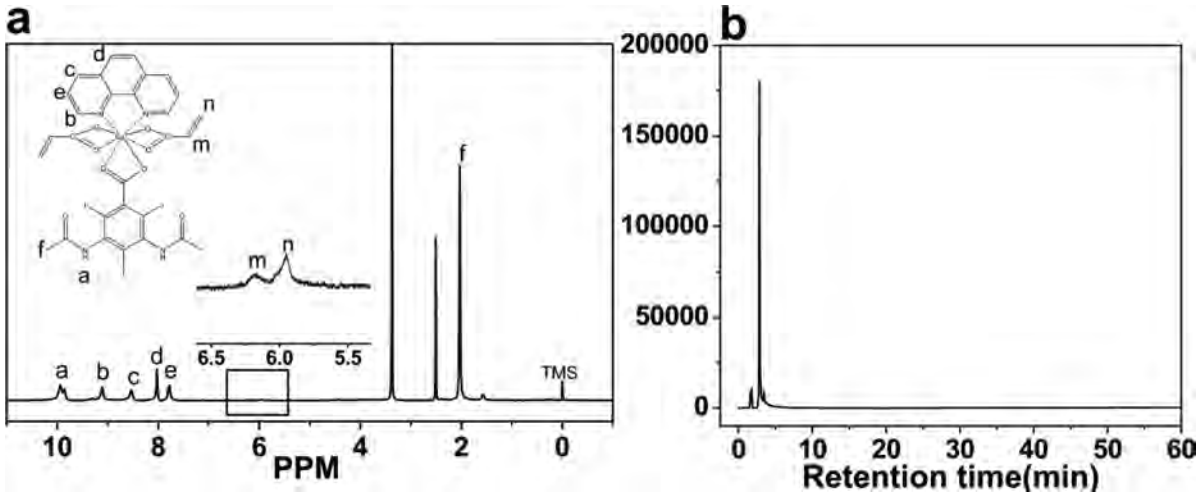

Figure 2. (a) ^{1}H NMR spectra of complex (a–f, correspondence between H in chemical structures and spectra) and (b) HPLC profile of complex.

TFNPs and drenched in 4% paraformaldehyde for 24 h. The tissues were placed in paraffin for histological analysis and optical imaging via ion staining with Prussian blue. Optical imaging was performed by confocal laser scanning microscopy (CLSM). The CLSM figures of the TFNPs in the liver and spleen were acquired on the Spectra Physics MaiTai HP tunable two-photon (690–1040 nm) laser confocal microscopy (Carl Zeiss LSM710).

2.8. Materials Characterization. The chemical structure of the complex was determined by ^{1}H NMR on the UNITY INVOA 600 MHz spectrometer (Varian, USA) with DMSO-d6 as the solvent. The purity and molecular weight of complex was obtained by high-performance liquid chromatography (HPLC, SHIMADZU LC-6AD, Japan) and electrospray ionization mass spectrometry system (ESI-MS, Thermo-Finnigan LCQ-Advantage, USA). The HPLC system was set up with a C18 column with the mobile phase of 50% CH_3CN/50% CH_3OH under the detection wavelength of 220 nm. The elemental analysis was performed on the elemental analyzer (Vario MICRO cube, Elementar, Germany), and XRF-1800 (WD-XRF, SHIMADZU, Japan). Fourier-transform infrared spectroscopy (FTIR) was conducted on complex, modified magnetic and TFNPs powders via the PerkinElmer Spectrum one Transform Infrared spectrometer (USA). The morphology of the TFNPs was observed by transmission electron microscopy (TEM, Tecnai G20, FEI Corp., USA) and scanning electron microscopy (SEM, JSM6510LV, JEOL, Japan). Prior to SEM, the diluted solution of TFNPs was dropped onto a glass slide, dried at room temperature, and vacuum metallized. The hydrodynamic size and size distribution of the TFNPs were measured by dynamic light scattering (DLS, Autosize Loc-Fc-963, Malvern Instrument). The X-ray diffraction (XRD, X'PertPro, Philips Corp., Nederland) spectra were acquired from the modified magnetic Fe_3O_4 nanoparticles and TFNPs using Cu Kα radiation at a scanning range between 20 and 80° (10°/min). Thermogravimetric analysis (TGA) was carried out by heating the powder of test samples on the PerkinElmer TGA-7 from 40 to 660 °C at a rate of 20 °C/min in a nitrogen atmosphere. The magnetic properties were determined on a vibrating sample magnetometer (VSM, HH-15, China) at 298 K under an applied magnetic field, and the fluorescence property of samples were obtained on the F-2500 spectrometer (Hitachi High Technologies Corporation, Japan). The Fe concentration in the TFNPs latex was acquired by inductively coupled plasma atomic emission spectrometry (ICP-AES, Optima 8000, PerkinElmer), and the sample was prepared by dissolving the nanoparticles in a solution of HNO_3 at 120 °C.

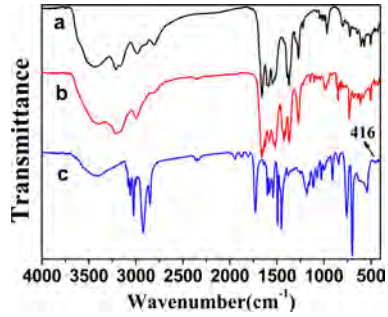

Figure 3. FTIR spectra: (a) DTA, (b) $Eu(AA)_2(DTA)Phen$, and (c) TFNPs.

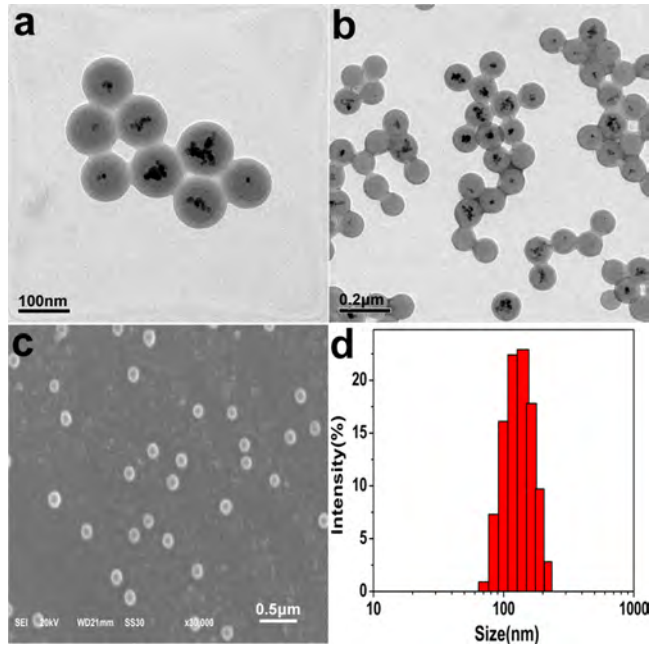

Figure 4. (a and b) TEM and (c) SEM images as well as (d) size distribution of the TFNPs.

3. RESULTS AND DISCUSSION

3.1. Synthesis and Characterization of Eu(III) Complex: $Eu(AA)_2(DTA)Phen$ and TFNPs. Figure 1 illustrates the synthesis procedures of the Eu(III) complex and TFNPs. The polymerizable iodine-containing rare-earth complex is synthesized using a coordination of DTA, $EuCl_3$, AA, and Phen. The modified magnetic Fe_3O_4 nanoparticles are obtained by modifying the Fe_3O_4 NPs with OA and NaUA (Fe_3O_4/(OA/

DOI: 10.1021/acsami.5b08802
ACS Appl. Mater. Interfaces 2015, 7, 24523–24532

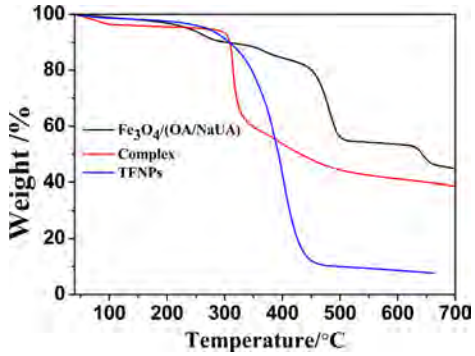

Figure 5. TGA curves of Fe_3O_4/(OA/NaUA), $Eu(AA)_2$(DTA)Phen, and TFNPs.

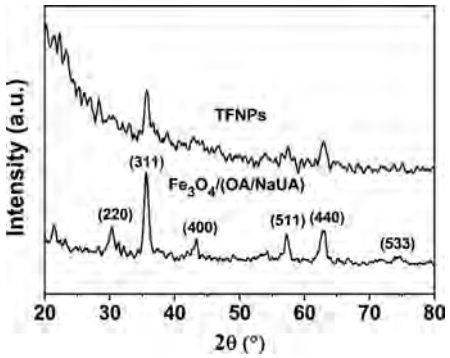

Figure 6. X-ray powder diffraction patterns of Fe_3O_4/(OA/NaUA) and TFNPs.

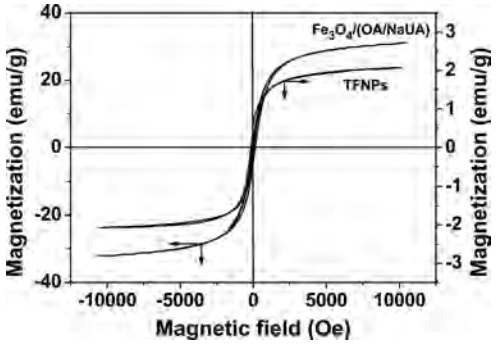

Figure 7. Magnetic hysteresis loops of the Fe_3O_4/(OA/NaUA) and TFNPs.

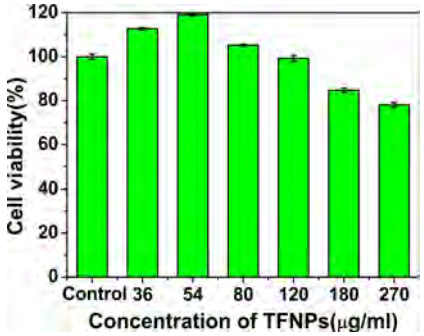

Figure 8. Cell viability of HeLa cells cocultivated with different concentrations of TFNPs in MTT assay.

NaUA)). St, GMA, and Fe_3O_4/(OA/NaUA) are added to water (dispersing solvent) in emulsifier-free emulsion polymerization in which the monomers diffuse into the hydrophobic layer formed by OA and NaUA under mechanical mixing. Polymerization via double bonds form the monomers and NaUA produced the core−shell Fe_3O_4/poly(St-GMA) seeds. Finally, the solution with the iodine-containing rare-earth complex is added, and the TFNPs are obtained by polymerization of the complex and the rest of monomers. The interlayer of the polymer can effectively reduce fluorescence quenching of the complex caused by the magnetic core.

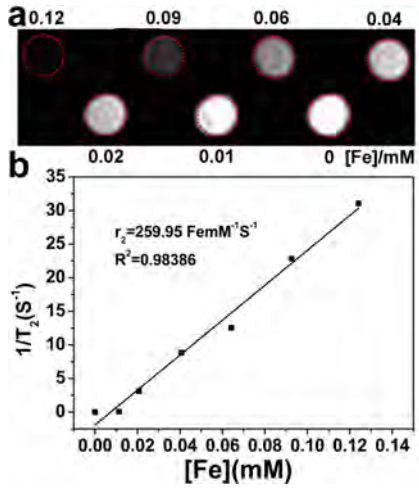

Figure 9. (a) T_2 weight MR images of the aqueous solution containing TFNPs with different iron concentrations and (b) T_2 relaxation rate ($1/T_2$) as a function of iron concentrations in the TFNPs.

The chemical structures of $Eu(AA)_2$(DTA)Phen determined by ^{1}H NMR in DMSO-d_6 are presented in Figure 2a. The characteristic signals of this complex are as follows: b, δ = 9.11 ppm, c, δ = 8.53 ppm, d, δ = 8.02 ppm, and e, δ = 7.79 ppm, belonging to Phen; a, δ = 9.94 ppm, and f, δ = 2.03 ppm, belonging to DTA; and the peak at 3.37 ppm, associated with water protons in the complex. The weak peaks n, δ = 5.91−6.04 ppm, and m, δ = 6.16−6.24 ppm, stem from the protons of $-CH_2{=}CH_2$ on AA, which have a signal expression in DMSO-d_6 lower than those in D_2O; nevertheless, the reactive hydrogen of −NHCO− on DTA will be invisible in D_2O. Thus, we utilize HPLC (Figure 2b) and ESI-MS (Figure S1) for further verification. The single peak on Figure 2b reflects purity of complex (93.4%). In Figure S1, the molecular weight of sample (1085.0 (100) $[M - H]^-$, calculated 1086.7), which is in accord with the theoretical value of the expected structure. The HPLC data of sodium diatrizoate hydrate and Phen are also provided as experimental controls in Figure S2.

The structure of the complex is further assessed by elemental analysis and WD-XRF. The weight ratios of C, H, and N in the complex as measured on the elemental analyzer are 31.94, 2.4, and 5.14%, which are in line with the theoretical values of 31.57, 2.3, and 4.78%. The relative mass ratios of Eu and I in the complex (Eu: 28.6732%, I: 71.3268%) as determined by WD-XRF are also consistent with those of the expected structure. The relative mass ratios of Fe, Eu, and I in the TFNPs based on WD-XRF are Fe: 80.8272%, Eu: 15.3082%, and I: 3.8647%, indicating successful aggregation of the complex in TFNPs.

The FTIR spectra of sodium diatrizoate hydrate, complex, and TFNPs are depicted in Figure 3. As shown in Figure 3b, the C═O stretching bands of AA at 1730 cm^{-1} are absent from the complex. The antisymmetric and symmetric stretching

DOI: 10.1021/acsami.5b08802
ACS Appl. Mater. Interfaces 2015, 7, 24523−24532

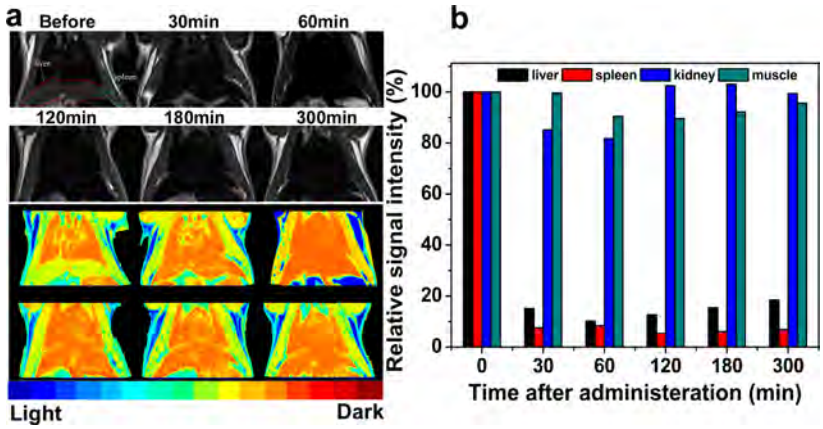

Figure 10. (a) T_2-weighted MR images of rats at different time points before and after injection of TFNPs. (b) Relative signal enhancement values of the liver, spleen, kidney, and muscle before and after injection of TFNPs.

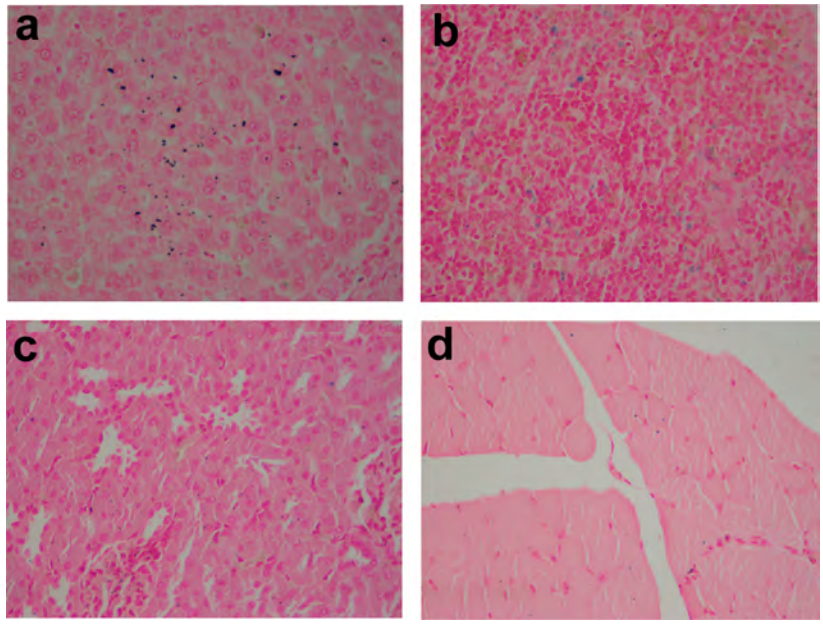

Figure 11. Prussian blue stained images (400×): (a) liver, (b) spleen, (c) kidney, and (d) muscle 9 h after tail vein injection of TFNPs.

vibrations of COO^- at 1543 and 1427 cm^{-1} and C═C vibration of AA at 1624 cm^{-1} indicate coordination of AA with the Eu ion. The peak at 1660 cm^{-1} corresponding to stretching vibration of C═O (acylamino) confirms that sodium diatrizoate hydrate coordinates with the Eu ion, whereas coordination of Phen is proven by the C═N stretching vibration and C−H bent vibration at 848 and 673 cm^{-1} in the complex, respectively. In the spectrum of the TFNPs (Figure 3c), the peak at 1729 cm^{-1} arises from the carbonyl groups in PGMA, and those at 842 and 907 cm^{-1} derive from the oxirane ring asymmetrical expansion and contraction vibrations. The flexural vibration (δ_{C-H}) peaks of the benzene ring from PSt are at 757 and 697 cm^{-1}. In addition, the peaks at 539 cm^{-1} correspond to the Fe−O vibration in Fe_3O_4 NPs, and that at 416 cm^{-1} is due to Eu−O vibration. These results indicate successful preparation of the trifunctional nanoparticle TFNPs.

The morphology of the TFNPs is shown in Figure 4. The hydrodynamic size of the TFNPs is about 130 nm with a polydispersity index (PDI) of 0.017. Meanwhile, the TFNPs show a good uniform dispersion according to TEM and a regular spherical structure as based on SEM. The majority of the TFNPs have a dark core with Fe_3O_4 NPs. Furthermore, the polymer shell between the Fe_3O_4 NPs and luminescent shell can effectively prevent fluorescence quenching.

The TGA curves of the modified magnetic Fe_3O_4 NPs, complex, and TFNPs in a nitrogen atmosphere are shown in Figure 5. The complex shows a weight loss of 3.6% at 100 °C because of the disappearance of crystal water from the complex. The thermal-decomposition temperature of the TFNPs is about 270 °C, thus revealing good thermal stability. The residue weight percentage of the TFNPs at 700 °C is about 7.66% because of the presence of Fe and Eu oxide.

The XRD spectra reveal the crystal structures of the modified magnetic Fe_3O_4 NPs and TFNPs. As shown in Figure 6, the Fe_3O_4/(OA/NaUA) NPs show the main peaks at 2θ of 30, 35, 43, 57, 62.5, and 74.5°, corresponding to the crystal plane indices of (220), (311), (400), (511), and (440). These peaks match the face-centered cubic Fe_3O_4 crystal structure of the reference inorganic crystal structure database (ICSD). The XRD pattern of the TFNPs is in accord with that of the Fe_3O_4 NPs, and the broad diffusion pattern at low 2θ indicates that

DOI: 10.1021/acsami.5b08802
ACS Appl. Mater. Interfaces 2015, 7, 24523−24532

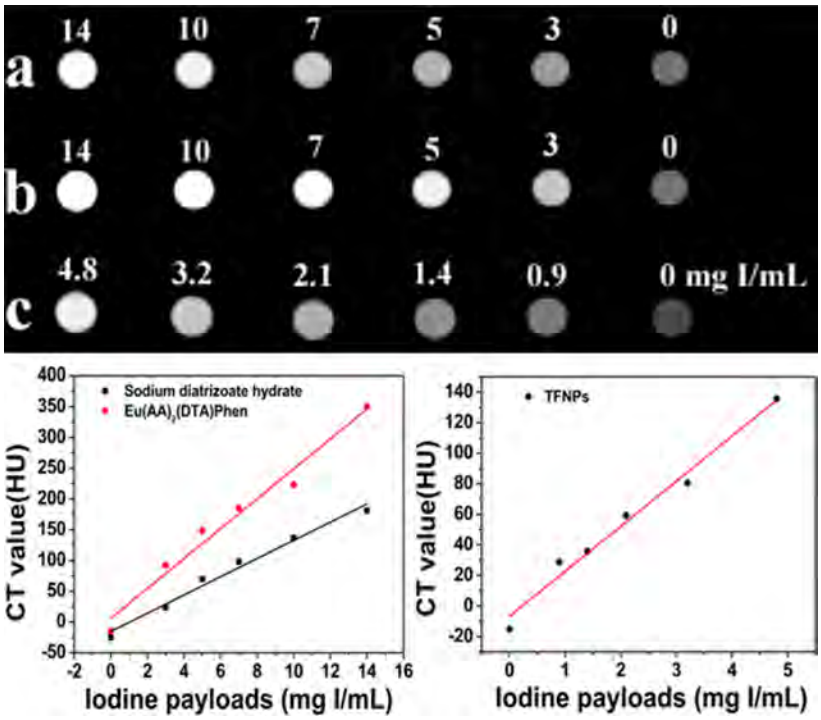

Figure 12. In vitro CT images: (a) sodium diatrizoate hydrate, (b) complex $Eu(AA)_2(DTA)Phen$, and (c) TFNPs and plots of corresponding CT value (HU) as a function of iodine payloads in a−c.

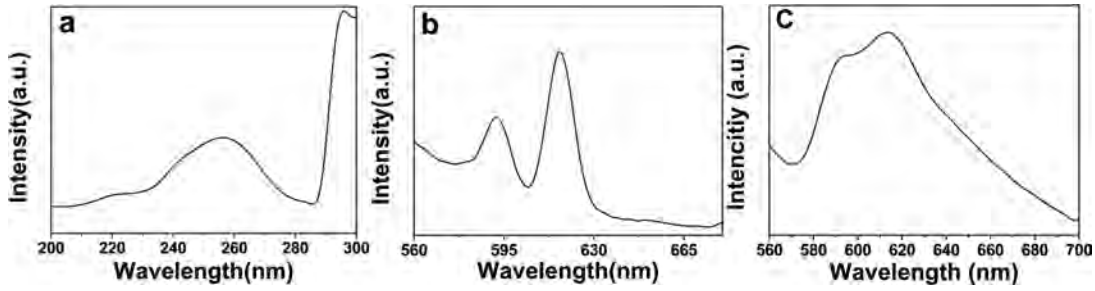

Figure 13. Excitation spectra of (a) TFNPs fixed-emission spectrum (λ_{em} = 619 nm). Emission spectra of (b) complex and (c) TFNPs fixed-excitation spectrum (λ_{ex} = 257 nm).

parts of the Fe_3O_4 particles are coated on the amorphous polymer layer.

Figure 7 displays the magnetic properties of TFNPs and Fe_3O_4/(OA/NaUA) magnetofluid characterized by the VSM at room temperature. Both samples show superparamagnetism with no magnetic remnants. The saturation magnetization values (M_s) of Fe_3O_4/(OA/NaUA) and TFNPs are 30.09 and 2.16 emu/g, respectively. The saturation magnetization of the TFNPs has a loss mainly because of the nonmagnetic polymer layer that reduces the total magnetization.

3.2. In Vitro Cytotoxicity. The MTT assay is applied to evaluate the in vitro cytotoxicity of TFNPs. The relative cell viability of the HeLa cells with different concentrations of TFNPs is shown in Figure 8. The cell viability is greater than 80% for most of the samples, and even if the concentration of TFNPs reaches 270 μg/mL, a cell viability higher than 70% can still be obtained. These results indicate that TFNPs would have good cell biocompatibility and thus may be suited to clinical applications in animal models.

3.3. In Vitro Relaxivity and in Vivo MRI. The feasibility of the TFNPs as a T_2 contrast agent is characterized by measuring the T_2 relaxation time and the T_2-weighted MR images of the TFNPs with different iron concentrations on a clinical 3T MR scanner. The MR images of the TFNPs solutions in Figure 9 show an obvious signal loss (concentration-dependent darkening). The precise effect of transverse relaxation is represented by the transverse relativity (r_2). The relationship of the inverse relaxation time $1/T_2$ versus iron concentrations is plotted in Figure 9b, and the linear fitting between $1/T_2$ and iron concentration is based on the following equation: $1/T_2 = 1/T_2^0 + r_2[Fe]$, where $1/T_2^0$ is the inverse relaxation time of deionized water and [Fe] is the iron concentration of TFNPs. The transverse relativity (r_2) of TFNPs is calculated to be 260 mM^{-1} s^{-1}, which is obviously higher than that of clinically used RESOVIST (132−154 mM^{-1} s^{-1}) and FERIDEX/ENDOREM (87−99 mM^{-1} s^{-1}).[42] This value also indicates a great potential of TFNPs as a T_2-weighted MRI contrast agent.

The in vivo T_2-weighted MR imaging capability of the TFNPs is evaluated using SD rats as the animal model. Figure 10a depicts the T_2-weighted MR images based on different time points after tail vein injection of the TFNPs, and the relative signal intensity is displayed in Figure 10b. The liver exhibits obvious darkening, and the minimum relative MRI signal intensity of 10.14% is observed 60 min after injection. The

DOI: 10.1021/acsami.5b08802
ACS Appl. Mater. Interfaces 2015, 7, 24523−24532

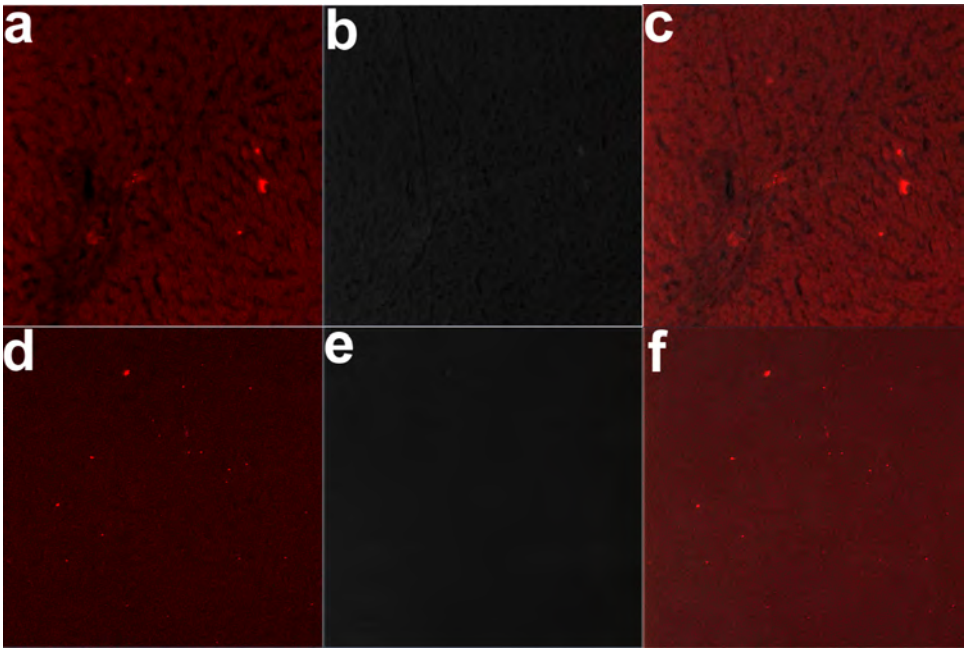

Figure 14. (a and b) CLSM images of liver under two-photon 690 nm laser irradiation and natural light. (c) Overlap image of a and b. (d and e) CLSM images of the spleen under two-photon 690 nm laser irradiation and natural light. (f) Overlap image of d and e.

relative SI from the liver is low between 15.12 and 18.47% at 30 to 300 min postinjection, and that from the kidney and muscle remains the same. The observation from the spleen is similar to that from the liver, indicating that most TFNPs are engulfed by macrophages of the reticuloendothelial system (RES) in the liver and spleen. The kidney and muscle show no significant changes because of the lack of macrophages.

The liver, spleen, kidney, and muscle of the SD rat undergo biopsy and are stained with Prussian blue at 9 h postinjection. As shown in Figure 11, the TFNPs manifest as blue dots and aggregate in the liver and spleen. However, blue dots are hardly observed from the kidney and muscle, indicating that the TFNPs are good T_2 contrast agents in these organs.

3.4. In Vitro CT Characterization. The clinical potential of the complex and TFNPs pertaining to CT imaging is evaluated as shown in Figure 12. Sodium diatrizoate hydrate is diluted with distilled water to obtain the same iodine payload as that of the solution of the complex, 14 mg I/mL. It is important to note that the iodine payload of the TFNPs is the ideal value, but the actual value is lower and difficult to determine exactly because of the loss of the complex during preparation and the small complex content. The main objective is to evaluation the functionality in CT imaging. The brightness of the CT images increases with iodine payload and the CT values (HU) increase linearly. In general, the complex exhibits better contrast than sodium diatrizoate hydrate with the same iodine payload. The latex of the TFNPs retains the obvious contrast effect at the iodine payload of 4.8 mg I/mL.

3.5. Luminescence Properties and in Vivo Optical Imaging. The fluorescence properties of the complex and TFNPs are determined by the excitation and emission spectra. Figure 13a displays the excitation spectra of the complex and TFNPs by setting the emission intensity of Eu(III) at 619 nm. Both samples show the same excitation peak at 257 nm because of the $\pi-\pi^*$ transitions of Phen. Figure 13b,c depicts the emission spectra of the complex and TFNPs excited by 257 nm. The peaks at 593 and 619 nm are the characteristic emission peaks of Eu(III) stemming from the $^5D_0 \rightarrow {}^7F_1$ and $^5D_0 \rightarrow {}^7F_2$ transitions. The emission spectra of TFNPs also indicate successful polymerization of the complex.

The in vivo optical properties of TFNPs are measured by analyzing the liver and spleen slices on two-photon laser confocal microscopy (Carl Zeiss LSM710, 690−1040 nm). The CLSM images are shown in Figure 14. The TFNPs exhibit characteristic vivid fluorescence dots under two-photon 690 nm laser irradiation (Figure 14a,d), but there is no fluorescence under natural light illumination (Figure 14b,e). Obvious fluorescence still is observed from the overlapping images using the two light sources (Figure 14c,f). The organic layer between the magnetic center and complex curbs fluorescence quenching in the TFNPs, thereby confirming the excellent fluorescent properties of the TFNPs as an optical probe in clinical applications.

4. CONCLUSIONS

An iodine-containing Eu(III) complex and TFNPs with multiple optical and imaging functionalities are synthesized under mild conditions. The TFNPs, which have a narrow size distribution with a hydrodynamic diameter of 130 nm, are effective MRI contrast agents. The Eu^{3+} ions in TFNPs exhibit characteristic red luminescence on CLSM imaging, and the complex shows better CT contrast effects for the same iodine payload as sodium diatrizoate hydrate. Both the TFNPs and complex deliver good CT contrast performance in vitro, suggesting their large potential in multifunctional biomedical applications. In particular, DTA just is a simple derivative of 1,3,5-triiodobenzene, which is derived from the currently most-used iodinated contrast agent. Therefore, we could directly use or simply modify more clinical CT contrast agents to develop polymerizable multiple functional CT contrast agents in the same way. These new types of polymerizable CT contrast agents also can use various chemical syntheses for more function and applied range than those included of emulsion

DOI: 10.1021/acsami.5b08802
ACS Appl. Mater. Interfaces 2015, 7, 24523−24532

polymerization in this paper. From this perspective, TFNPs and the complex are worth further research.

■ ASSOCIATED CONTENT

Supporting Information

The Supporting Information is available free of charge on the ACS Publications website at DOI: 10.1021/acsami.5b08802.

ESI-MS spectra of complex and HPLC measurement of sodium diatrizoate hydrate and Phen. (PDF)

■ AUTHOR INFORMATION

Corresponding Authors

*E-mail: zushunxu@hubu.edu.cn.

*E-mail: xuhaibo1120@hotmail.com.

*Tel.: +852 34427724. Fax: +852 34420542. E-mail: paul.chu@cityu.edu.hk.

Author Contributions

X.W. and M.T. contributed equally to this project.

Notes

The authors declare no competing financial interest.

■ ACKNOWLEDGMENTS

The work was financially supported by the National Natural Science Foundation of China (grant nos. 51573039, 81171386, and 81372369) and also in part by National 973 Program of China (grant no. 2011CB933103), City University of Hong Kong Strategic Research Grant (SRG) no. 7004188, and Hong Kong Research Grants Council (RGC) General Research Funds (GRF) no. CityU 112.

■ REFERENCES

(1) Della Rocca, J.; Lin, W. Nanoscale Metal-organic Frameworks: Magnetic Resonance Imaging Contrast Agents and Beyond. *Eur. J. Inorg. Chem.* **2010**, *2010*, 3725−3734.

(2) Zeng, S.; Tsang, M. K.; Chan, C. F.; Wong, K. L.; Hao, J. PEG Modified $BaGdF_5$:Yb/Er Nanoprobes for Multi-modal Upconversion Fluorescent, in Vivo X-ray Computed Tomography and Biomagnetic Imaging. *Biomaterials* **2012**, *33*, 9232−9238.

(3) Feng, S. T.; Wang, M.; Gao, Z.; Tan, G.; Cai, H.; Hu, X.; Yang, J.; Li, Z. P. The Influence of Upper Limb Position on the Effect of a Contrast Agent in Chest CT Enhancement. *Eur. J. Radiol.* **2013**, *82*, 1023−1027.

(4) Iavarone, M.; Piscaglia, F.; Vavassori, S.; Galassi, M.; Sangiovanni, A.; Venerandi, L.; Forzenigo, L. V.; Golfieri, R.; Bolondi, L.; Colombo, M. Contrast Enhanced CT-scan to Diagnose Intrahepatic Cholangiocarcinoma in Patients with Cirrhosis. *J. Hepatol.* **2013**, *58*, 1188−1193.

(5) Buchbender, C.; Hartung-Knemeyer, V.; Beiderwellen, K.; Heusch, P.; Kuhl, H.; Lauenstein, T. C.; Forsting, M.; Antoch, G.; Heusner, T. A. Diffusion-weighted Imaging as Part of Hybrid PET/MRI Protocols for Whole-body Cancer Staging: Does It Benefit Lesion Detection? *Eur. J. Radiol.* **2013**, *82*, 877−882.

(6) Kircher, M. F.; Willmann, J. K. Molecular Body Imaging: MR Imaging, CT, and US. Part I. Principles. *Radiology* **2012**, *263*, 633−643.

(7) Aillon, K. L.; El-Gendy, N.; Dennis, C.; Norenberg, J. P.; McDonald, J.; Berkland, C. Iodinated Nanoclusters as an Inhaled Computed Tomography Contrast Agent for Lung Visualization. *Mol. Pharmaceutics* **2010**, *7*, 1274−1282.

(8) Fu, Y.; Nitecki, D.; Maltby, D.; Simon, G. H.; Berejnoi, K.; Raatschen, H. J.; Yeh, B. M.; Shames, D. M.; Brasch, R. C. Dendritic Iodinated Contrast Agents with PEG-cores for CT Imaging: Synthesis and Preliminary Characterization. *Bioconjugate Chem.* **2006**, *17*, 1043−1056.

(9) Lee, N.; Choi, S. H.; Hyeon, T. Nano-sized CT Contrast Agents. *Adv. Mater.* **2013**, *25*, 2641−2660.

(10) Chen, Q.; Li, K.; Wen, S.; Liu, H.; Peng, C.; Cai, H.; Shen, M.; Zhang, G.; Shi, X. Targeted CT/MR Dual Mode Imaging of Tumors Using Multifunctional Dendrimer-entrapped Gold Nanoparticles. *Biomaterials* **2013**, *34*, 5200−5209.

(11) Ai, K.; Liu, Y.; Liu, J.; Yuan, Q.; He, Y.; Lu, L. Large-scale Synthesis of Bi_2S_3 Nanodots as a Contrast Agent for in Vivo X-ray Computed Tomography Imaging. *Adv. Mater.* **2011**, *23*, 4886−4891.

(12) Torres, A. S.; Bonitatibus, P. J.; Colborn, R. E.; Goddard, G. D.; FitzGerald, P. F.; Lee, B. D.; Marino, M. E. Biological Performance of a Size-fractionated Core-shell Tantalum Oxide Nanoparticle X-ray Contrast Agent. *Invest. Radiol.* **2012**, *47*, 578−587.

(13) Liu, Z.; Li, Z.; Liu, J.; Gu, S.; Yuan, Q.; Ren, J.; Qu, X. Long-circulating Er^{3+}-doped Yb_2O_3 Up-conversion Nanoparticle as an in Vivo X-Ray CT Imaging Contrast Agent. *Biomaterials* **2012**, *33*, 6748−6757.

(14) Xing, H.; Bu, W.; Ren, Q.; Zheng, X.; Li, M.; Zhang, S.; Qu, H.; Wang, Z.; Hua, Y.; Zhao, K.; Zhou, L.; Peng, W.; Shi, J. A NaYbF4: Tm^{3+} Nanoprobe for CT and NIR-to-NIR Fluorescent Bimodal Imaging. *Biomaterials* **2012**, *33*, 5384−5393.

(15) de Vries, A.; Custers, E.; Lub, J.; van den Bosch, S.; Nicolay, K.; Grull, H. Block-copolymer-stabilized Iodinated Emulsions for Use as CT Contrast Agents. *Biomaterials* **2010**, *31*, 6537−6544.

(16) deKrafft, K. E.; Xie, Z.; Cao, G.; Tran, S.; Ma, L.; Zhou, O. Z.; Lin, W. Iodinated Nanoscale Coordination Polymers as Potential Contrast Agents for Computed Tomography. *Angew. Chem.* **2009**, *121*, 10085−10088.

(17) Galperin, A.; Margel, D.; Baniel, J.; Dank, G.; Biton, H.; Margel, S. Radiopaque Iodinated Polymeric Nanoparticles for X-ray Imaging Applications. *Biomaterials* **2007**, *28*, 4461−4468.

(18) Aviv, H.; Bartling, S.; Kieslling, F.; Margel, S. Radiopaque Iodinated Copolymeric Nanoparticles for X-ray Imaging Applications. *Biomaterials* **2009**, *30*, 5610−5616.

(19) Yan, K.; Li, H.; Li, P.; Zhu, H.; Shen, J.; Yi, C.; Wu, S.; Yeung, K. W.; Xu, Z.; Xu, H.; Chu, P. K. Self-assembled Magnetic Fluorescent Polymeric Micelles for Magnetic Resonance and Optical Imaging. *Biomaterials* **2014**, *35*, 344−355.

(20) Villaraza, A. J. L.; Bumb, A.; Brechbiel, M. W. Macromolecules, Dendrimers, and Nanomaterials in Magnetic Resonance Imaging: the Interplay between Size, Function, and Pharmacokinetics. *Chem. Rev.* **2010**, *110*, 2921−2959.

(21) Li, Y.; Laurent, S.; Esser, L.; Elst, L. V.; Muller, R. N.; Lowe, A. B.; Boyer, C.; Davis, T. P. The Precise Molecular Location of Gadolinium Atoms has a Significant Influence on the Efficacy of Nanoparticulate MRI Positive Contrast Agents. *Polym. Chem.* **2014**, *5*, 2592−2601.

(22) Gong, P.; Chen, Z.; Chen, Y.; Wang, W.; Wang, X.; Hu, A. High-relaxivity MRI Contrast Agents Prepared from Miniemulsion Polymerization using Gadolinium(III)-based Metallosurfactants. *Chem. Commun.* **2011**, *47*, 4240−4242.

(23) Loving, G. S.; Mukherjee, S.; Caravan, P. Redox-activated Manganese-based MR Contrast Agent. *J. Am. Chem. Soc.* **2013**, *135*, 4620−4623.

(24) Sun, M.; Zhang, H. Y.; Liu, B. W.; Liu, Y. Construction of a Supramolecular Polymer by Bridged Bis(permethyl-β-cyclodextrin)s with Porphyrins and Its Highly Efficient Magnetic Resonance Imaging. *Macromolecules* **2013**, *46*, 4268−4275.

(25) Gu, J.; Zhang, W.; Yang, X. Preparation of a Superparamagnetic MRI Contrast Agent with a Tumor Targeting Function. *Mater. Lett.* **2013**, *94*, 8−10.

(26) Lee, H.; Yu, M. K.; Park, S.; Moon, S.; Min, J. J.; Jeong, Y. Y.; Kang, H. W.; Jon, S. Thermally Cross-linked Superparamagnetic Iron Oxide Nanoparticles: Synthesis and Application as a Dual Imaging Probe for Cancer in Vivo. *J. Am. Chem. Soc.* **2007**, *129*, 12739−12745.

(27) Zhu, H.; Shang, Y.; Wang, W.; Zhou, Y.; Li, P.; Yan, K.; Wu, S.; Yeung, K. W.; Xu, Z.; Xu, H.; Chu, P. K. Fluorescent Magnetic Fe_3O_4/rare Earth Colloidal Nanoparticles for Dual-modality Imaging. *Small* **2013**, *9*, 2991−3000.

DOI: 10.1021/acsami.5b08802
ACS Appl. Mater. Interfaces 2015, 7, 24523−24532

(28) Qiao, R.; Jia, Q.; Hüwel, S.; Xia, R.; Liu, T.; Gao, F.; Galla, H. J.; Gao, M. Receptor-mediated Delivery of Magnetic Nanoparticles across the Blood-Brain Barrier. *ACS Nano* **2012**, *6*, 3304−3310.
(29) Zhong, Y.; Dai, F.; Deng, H.; Du, M.; Zhang, X.; Liu, Q.; Zhang, X. A Rheumatoid Arthritis Magnetic Resonance Imaging Contrast Agent based on Folic Acid Conjugated PEG-b-PAA@SPION. *J. Mater. Chem. B* **2014**, *2*, 2938−2946.
(30) Yan, K.; Li, H.; Wang, X.; Yi, C.; Zhang, Q.; Xu, Z.; Xu, H.; Whittaker, A. K. Self-assembled Magnetic Luminescent Hybrid Micelles Containing Rare Earth Eu for Dual-modality MR and Optical Imaging. *J. Mater. Chem. B* **2014**, *2*, 546−555.
(31) Shokrollahi, H. Contrast Agents for MRI. *Mater. Sci. Eng., C* **2013**, *33*, 4485−4497.
(32) Kwon, S.; Singh, R. K.; Kim, T. H.; Patel, K. D.; Kim, J. J.; Chrzanowski, W.; Kim, H. W. Luminescent Mesoporous Nanoreservoirs for the Effective Loading and Intracellular Delivery of Therapeutic Drugs. *Acta Biomater.* **2014**, *10*, 1431−1442.
(33) Yang, L.; Ding, Y.; Yang, Y.; Yan, Y.; Huang, J.; de Keizer, A.; Cohen Stuart, M. A. Fluorescence Enhancement by Microphase Separation-induced Chain Extension of Eu^{3+} Coordination Polymers: Phenomenon and Analysis. *Soft Matter* **2011**, *7*, 2720−2724.
(34) Zhang, Y.; Pan, S.; Teng, X.; Luo, Y.; Li, G. Bifunctional Magnetic-Luminescent Nanocomposites: Y_2O_3/Tb Nanorods on the Surface of Iron Oxide/Silica Core-Shell Nanostructures. *J. Phys. Chem. C* **2008**, *112*, 9623−9626.
(35) Hu, X. X.; Li, P. H.; Yeung, K. W. K.; Chu, P. K.; Wu, S. L.; Xu, Z. S. Synthesis and Characterization of Fluorescent Copolymer Containing Rare Earth Metal Complex and its Interaction with DNA. *J. Polym. Sci., Part A: Polym. Chem.* **2010**, *48*, 5961−5967.
(36) Torres Martin de Rosales, R.; Tavare, R.; Paul, R. L.; Jauregui-Osoro, M.; Protti, A.; Glaria, A.; Varma, G.; Szanda, I.; Blower, P. J. Synthesis of ^{64}Cu(II)-bis(dithiocarbamatebisphosphonate) and its Conjugation with Superparamagnetic Iron Oxide Nanoparticles: in Vivo Evaluation as Dual-modality PET-MRI Agent. *Angew. Chem., Int. Ed.* **2011**, *50*, 5509−5513.
(37) Bieze, M.; Klumpen, H. J.; Verheij, J.; Beuers, U.; Phoa, S. S.; van Gulik, T. M.; Bennink, R. J. Diagnostic Accuracy of ^{18}F-methylcholine Positron Emission Tomography/computed Tomography for Intra- and Extrahepatic Hepatocellular Carcinoma. *Hepatology* **2014**, *59*, 996−1006.
(38) Xing, H.; Bu, W.; Zhang, S.; Zheng, X.; Li, M.; Chen, F.; He, Q.; Zhou, L.; Peng, W.; Hua, Y.; Shi, J. Multifunctional Nanoprobes for Upconversion Fluorescence, MR and CT Trimodal Imaging. *Biomaterials* **2012**, *33*, 1079−1089.
(39) Xiao, Q.; Bu, W.; Ren, Q.; Zhang, S.; Xing, H.; Chen, F.; Li, M.; Zheng, X.; Hua, Y.; Zhou, L.; Peng, W.; Qu, H.; Wang, Z.; Zhao, K.; Shi, J. Radiopaque Fluorescence-transparent TaOx Decorated Upconversion Nanophosphors for in Vivo CT/MR/UCL Trimodal Imaging. *Biomaterials* **2012**, *33*, 7530−7539.
(40) Lusic, H.; Grinstaff, M. W. X-ray-computed Tomography Contrast Agents. *Chem. Rev.* **2013**, *113*, 1641−1666.
(41) Zhu, H.; Tao, J.; Wang, W.; Zhou, Y.; Li, P.; Li, Z.; Yan, K.; Wu, S.; Yeung, K. W.; Xu, Z.; Xu, H.; Chu, P. K. Magnetic, Fluorescent, and Thermo-responsive Fe_3O_4/rare Earth Incorporated Poly(St-NIPAM) Core-shell Colloidal Nanoparticles in Multimodal Optical/magnetic Resonance Imaging Probes. *Biomaterials* **2013**, *34*, 2296−2306.
(42) Rohrer, M.; Bauer, H.; Mintorovitch, J.; Requardt, M.; Weinmann, H. J. Comparison of Magnetic Properties of MRI Contrast Media Solutions at Different Magnetic Field Strengths. *Invest. Radiol.* **2005**, *40*, 715−724.

DOI: 10.1021/acsami.5b08802
ACS Appl. Mater. Interfaces 2015, 7, 24523−24532

Supporting information

of

Trifunctional Polymeric Nanocomposites Incorporated with Fe_3O_4/Iodine-Containing Rare Earth Complex for Computed X-ray Tomography, Magnetic Resonance, and Optical Imaging

Xin Wang,[†] Mengqi Tu,[‡] Kai Yan,[†] Penghui Li,[§] Long Pang,[†] Ying Gong,[†] Qing Li,[†] Ruiqing Liu,[†] Zushun Xu,*[,†] Haibo Xu,*[,‡] and Paul K. Chu*[,§]

[†]Hubei Collaborative Innovation Center for Advanced Organic Chemical Materials, Ministry of Education Key Laboratory for The Green Preparation and Application of Functional Materials, Hubei University , Wuhan, Hubei 430062, China

[‡]Department of Radiology, Union Hospital, Tongji Medical College, Huazhong University of Science and Technology, Wuhan, Hubei 430030, China

[§]Department of Physics and Materials Science, City University of Hong Kong, Tat Chee Avenue, Kowloon, Hong Kong, China

* Corresponding author:

Tel.: +852 34427724. fax: +852 34420542.

E-mail: zushunxu@hubu.edu.cn (Z. Xu),

E-mail: xuhaibo1120@hotmail.com (H. Xu),

E-mail: paul.chu@cityu.edu.hk (P. K. Chu)

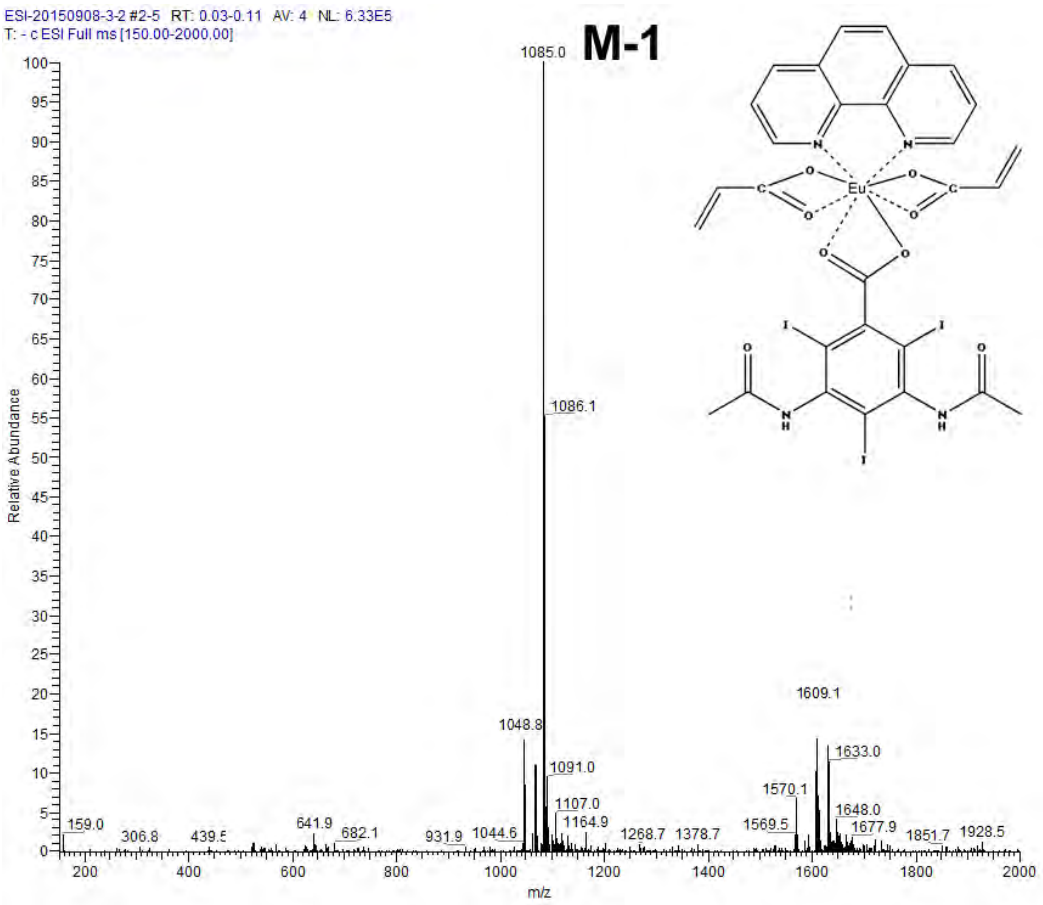

Figure S1. ESI-MS spectra of $Eu(AA)_2(DTA)Phen$

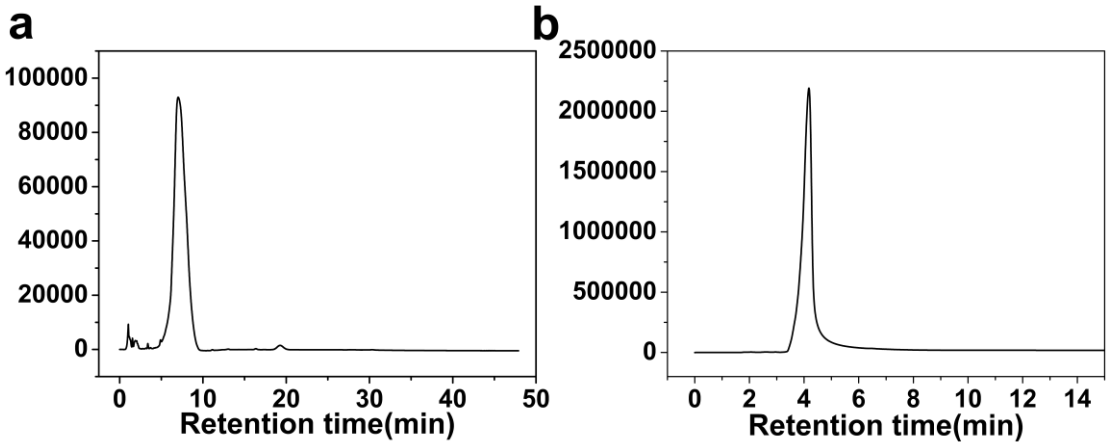

Figure S2. HPLC profile of (a) sodium diatrizoate hydrate and (b) Phen